Supporting Information

Potassium- and Rubidium-Passivated Alloyed Perovskite Films: Optoelectronic Properties and Moisture Stability

Mojtaba Abdi-Jalebi[1], *Zahra Andaji-Garmaroudi*[1], *Andrew J. Pearson*[1], *Giorgio Divitini*[2], *Stefania Cacovich*[2], *Bertrand Philippe*[3], *Håkan Rensmo*[3], *Caterina Ducati*[2], *Richard H. Friend*[1], *Samuel D. Stranks*[1]*

[1]Cavendish Laboratory, Department of Physics, University of Cambridge, Cambridge CB3 0HE, UK

[2]Department of Materials Science & Metallurgy, University of Cambridge, Cambridge CB3 0FS, UK

[3]Department of Physics and Astronomy, Uppsala University, Box 516, 75120 Uppsala, Sweden

*Corresponding author: sds65@cam.ac.uk

Materials and Methods

Film and device fabrication. We purchased the organic cation salts from Dyesol; the Pb compounds from TCI and CsI and KI from Alfa Aesar. Spiro-OMeTAD was purchased from Borun Chemicals and used as received. Unless otherwise stated, all other materials were purchased from Sigma-Aldrich.

We prepared the triple-cation-based perovskite $Cs_{0.06}FA_{0.79}MA_{0.15}Pb(I_{0.85}Br_{0.15})_3$ films by mixing PbI_2 (1.2 mol.L^{-1}), FAI (1.11 mol.L^{-1}), MABr (0.21 mol.L^{-1}) and $PbBr_2$ (0.21 mol.L^{-1}) in a mixture of anhydrous DMF:DMSO (4:1, volume ratio). We then added 5 volume percent CsI stock solution (1.5 mol.L^{-1} in DMSO) to the prepared double cation perovskite solution. The potassium iodide and rubidium iodide powders were first dissolved in mixed solutions of DMF/DMSO (4:1, volume ratios) to make stock solutions each of 1.5 mol.L^{-1}. The resulting KI and RbI solutions were added into the triple cation perovskite solution in different volume ratios to achieve the desired additive ratios. We then deposited the perovskite films by spin-coating the prepared solutions using a two-step program at 2000 and 6000 rpm for 10 and 30 seconds, respectively, and dripping 150 µL of chlorobenzene 30 seconds after the start of the spinning process. We then annealed the films at 100^{o}C for 60 minutes. We prepared all solutions and films in a nitrogen-filled glove box. For solar cell fabrication, we followed the same procedures for substrate preparation as well as deposition of both electron and hole transport layers (i.e. TiO_2, Spiro-OMeTAD with additives) as in our earlier works[1-2].

Photoluminescence characterization. Photoluminescence quantum efficiency (PLQE) measurements were taken by mounting perovskite films in an integrating sphere and photoexciting with a 532-nm continuous-wave laser at the given intensity. The laser and the emission signals were measured and quantified using a calibrated Andor iDus DU490A InGaAs detector for the determination of PL quantum efficiency. The PLQE was calculated as per de Mello et al[3].

Solar cell characterisation. Current–voltage characteristics were recorded by applying an external potential bias to the cell while recording the generated photocurrent with a digital source meter (Keithley Model 2400). The light source was a 450 - W xenon lamp (Oriel) equipped with a Schott-K113 Tempax sunlight filter (Praezisions Glas & OptikGmbH) to match the emission spectrum of the lamp to the AM1.5G standard. Before each measurement, the exact light intensity was determined using a calibrated Si reference diode equipped with an infrared cut-off filter (KG-3, Schott). All measurements were conducted using a non-reflective metal aperture of 0.105 cm^2 to define the active area of the device.

Scanning Transmission Electron Microscopy-Energy Dispersive X-ray Spectroscopy (STEM-EDX). A FEI Helios Nanolab dual beam Focus Ion Beam / Field Emission Gun - Scanning Electron Microscope (FIB/FEGSEM) was employed to prepare lamellae for STEM imaging and analysis. To preserve the perovskite film during specimen preparation, capping layers of Spiro-OMeTAD and platinum were deposited. All imaging was carried out in STEM-HAADF (High Angle Annular Dark Field) mode. STEM/EDX data were acquired in a FEI Tecnai Osiris TEM equipped with a high brightness Schottky X-FEG gun and a Super-X EDX system composed by four silicon drift detectors, each approximately 30 mm^2 in area and placed symmetrically around the optic axis to achieve a collection solid angle of 0.9 sr. Spectrum images were acquired with a probe current of 0.6 nA, an acceleration voltage of 200 kV, a spatial sampling of 10 or 20 nm/pixel for medium and low magnification maps respectively, and 50 ms/pixel dwell time. Data were acquired with Tecnai Imaging and Analysis (TIA) and analysed with Hyperspy.

Photoelectron spectroscopy. Photoelectron spectroscopy (PES) was performed through a methodology described in a previous work[4]. In short, a combination of in-house X-ray Photoelectron Spectroscopy (XPS) and Hard X-ray Photoelectron Spectroscopy (HAXPES) were performed in this work. XPS measurements were done with a Scienta ESCA 300

instrument, using monochromatized AlKα radiation (hν=1486.6 eV). HAXPES was carried out at BESSY II (Helmholtz Zentrum Berlin, Germany) at the KMC-1 beamline using the HIKE end-station. To obtain a deeper depth level than that of classical XPS, an incident photon energy of 4000 eV was used by selecting the first-order light from a Si(311) crystal of a double-crystal monochromator (Oxford-Danfysik). Calibration was done by measuring a gold plate reference and setting the Au $4f_{7/2}$ core level peak to 84.0 eV, corresponding to a zero binding energy at the Fermi level. The samples investigated by XPS and HAXPES were the same and stored in a sealed box with common desiccants to limit moisture contamination.

Scanning Electron Microscopy. The surface morphology of the films was examined using an FESEM (Merlin). An electron beam accelerated to 3 kV was used with an in-lens detector. EDX was carried out on a FEI Nova NanoSEM at 10kV acceleration voltage using a Bruker XFlash 6 detector. The maps were processed within Esprit 2.1 and Hyperspy.

X-ray diffraction. XRD was performed using a Bruker X-ray D8 Advance diffractometer with Cu $K\alpha_{1,2}$ radiation (λ = 1.541 Å). Spectra were collected with an angular range of $5 < 2\theta < 60$ º and $\Delta\theta = 0.01227$ º over 10 minutes. Ageing treatments were performed in dark conditions using a dedicated sample chamber with continuous humid N_2 flow and controlled relative humidity.

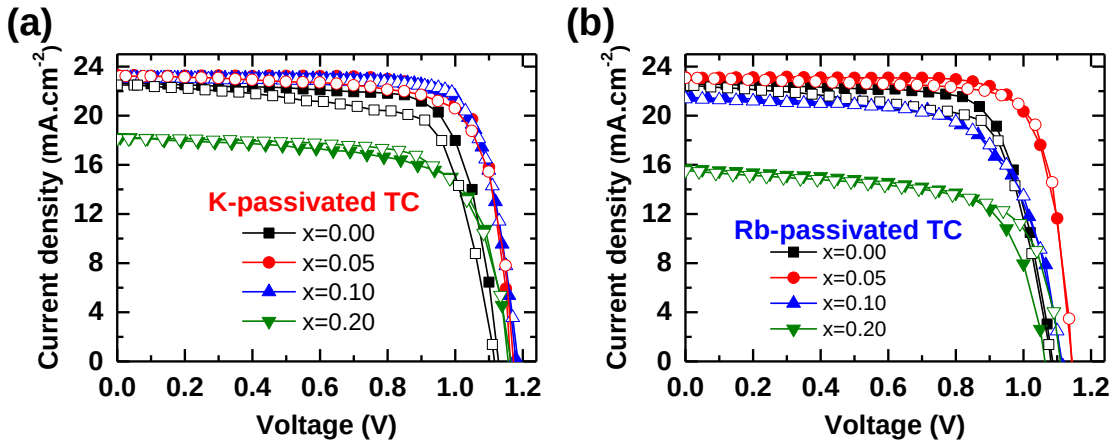

Figure S1. Reverse (closed symbols) and forward (open symbols) current density-voltage characteristics of perovskite solar cells for different loadings (*x*) of passivation agents (a) K and (b) Rb into the TC perovskite layers. The scans were measured under full-simulated solar illumination conditions (AM1.5, 100 mW.cm^{-2}) and scanned at a rate of 15 mV/s.

Table S1. Device photovoltaic parameters extracted from Figure S1 for different loadings of passivation agents K (upper) and Rb (lower) into the TC perovskites measured under full-simulated solar illumination conditions (AM1.5, 100 mW.cm^{-2}) and scanned at a rate of 15 mV/s.

Sample	*x*		J_{sc} [mA.cm^{-2}]	V_{oc} [V]	FF	PCE [%]
K-passivated TC	**0.00**	Reverse	22.65	1.07	0.75	18.2
		Forward	22.48	1.06	0.71	16.9
	0.05	Reverse	23.25	1.17	0.77	20.9
		Forward	23.22	1.17	0.76	20.6
	0.10	Reverse	23.06	1.18	0.79	21.6
		Forward	23.09	1.19	0.79	21.7
	0.20	Reverse	18.24	1.16	0.70	14.8
		Forward	18.14	1.16	0.71	14.9
Rb-passivated TC	**0.00**	Reverse	22.58	1.09	0.74	18.1
		Forward	22.47	1.08	0.71	17.2
	0.05	Reverse	23.11	1.14	0.78	20.6
		Forward	23.07	1.14	0.79	20.7
	0.10	Reverse	21.48	1.12	0.67	16.1
		Forward	21.36	1.11	0.67	16.0
	0.20	Reverse	15.83	1.11	0.64	11.3
		Forward	15.53	1.10	0.67	11.5

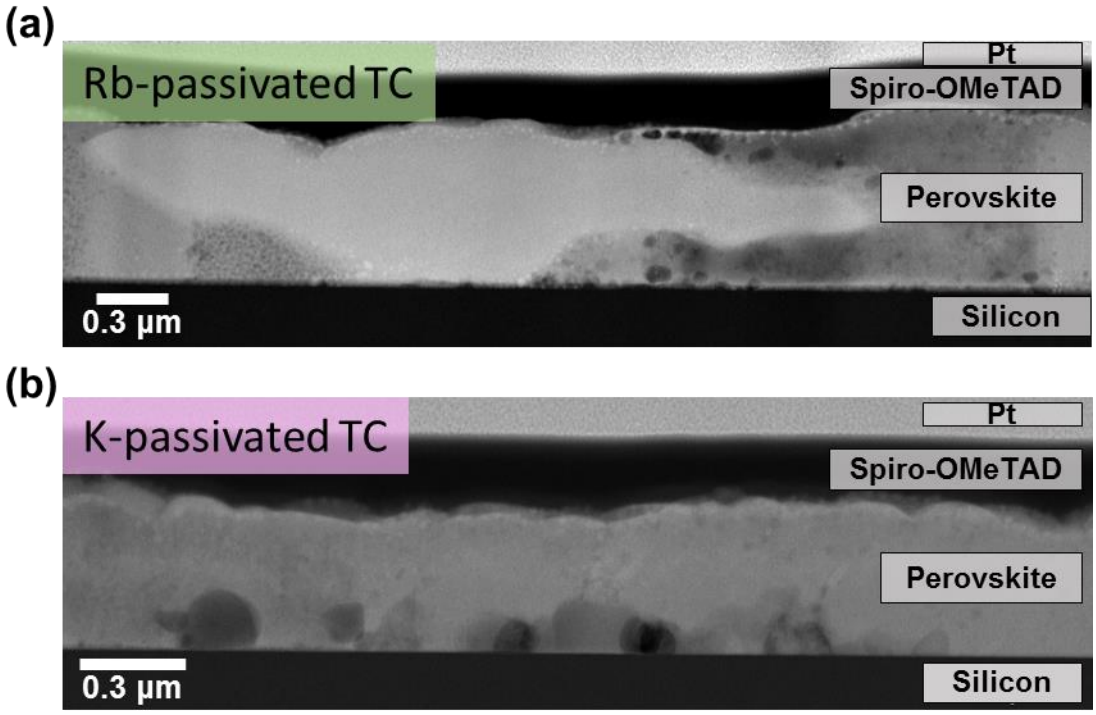

Figure S2. HAADF STEM cross sectional images of (a) Rb-passivated TC and (b) K-passivated TC deposited on silicon substrates with Spiro-OMeTAD and platinum capping layers to preserve the perovskite layer during lamella preparation.

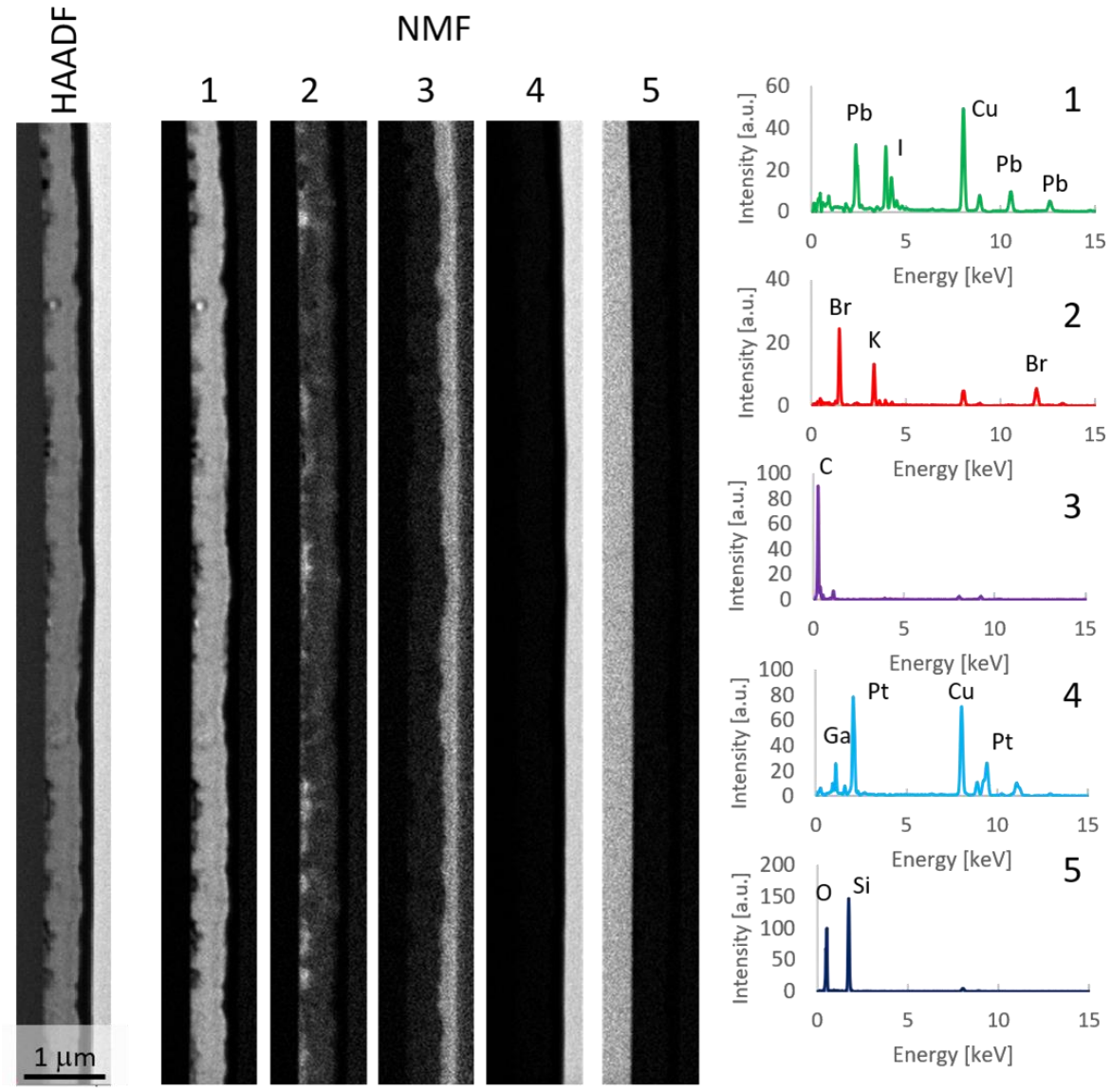

Figure S3. STEM-HAADF reference image and NMF decomposition results for the K-passivated TC sample. For each component, a spatial distribution is shown on the left and the corresponding profile is displayed on the right. Components can be identified as perovskite (1), Br-K phase (2), Spiro (3), Pt/Ga capping from FIB preparation (4) and substrate (5).

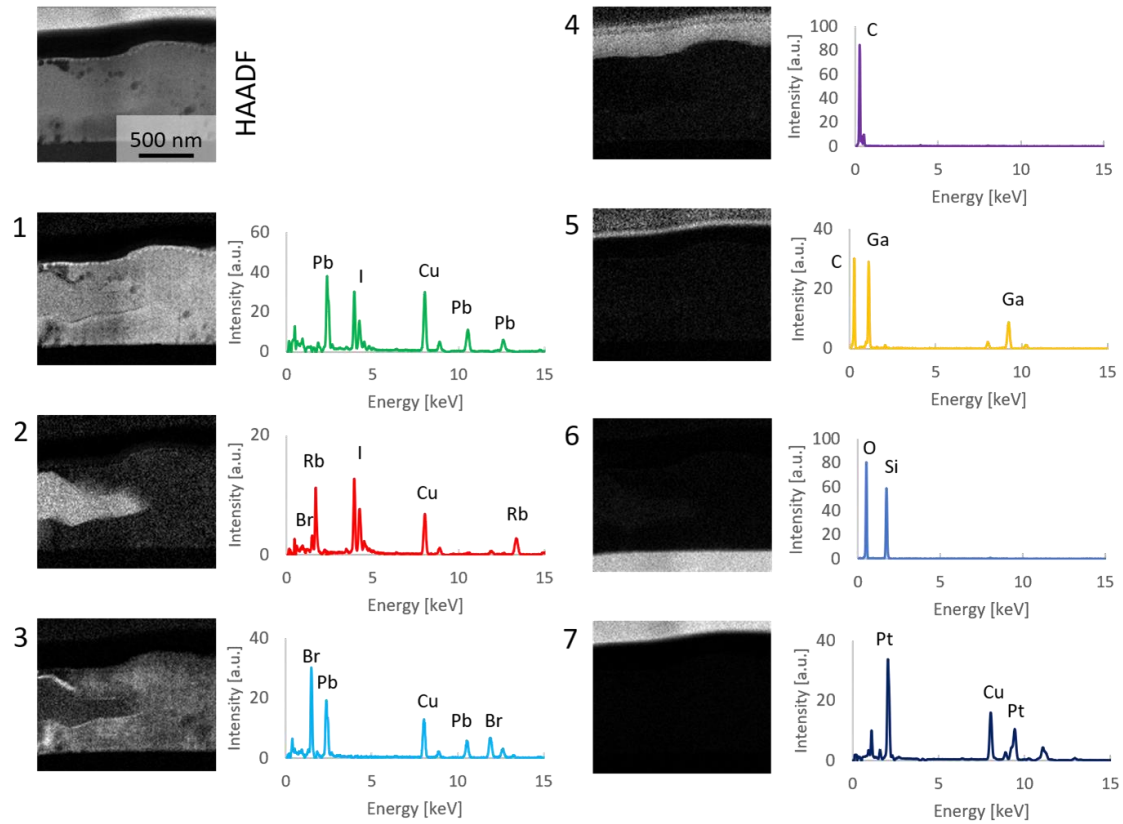

Figure S4. STEM-HAADF reference image and NMF decomposition results for the Rb-passivated TC sample. For each component, a spatial distribution is shown on the left and the corresponding profile is displayed on the right. The main perovskite phase is described by component 1 (green). Component 2 (red) indicates the presence of a separate phase, containing Rb, I, and Br, located in a grain. Component 3 (light blue) describes the relatively inhomogeneous distribution of Br within the perovskite. The other components can be identified as Spiro (4), implanted Ga from the FIB sample preparation (5), silicon oxide as substrate (6) and Pt capping (7).

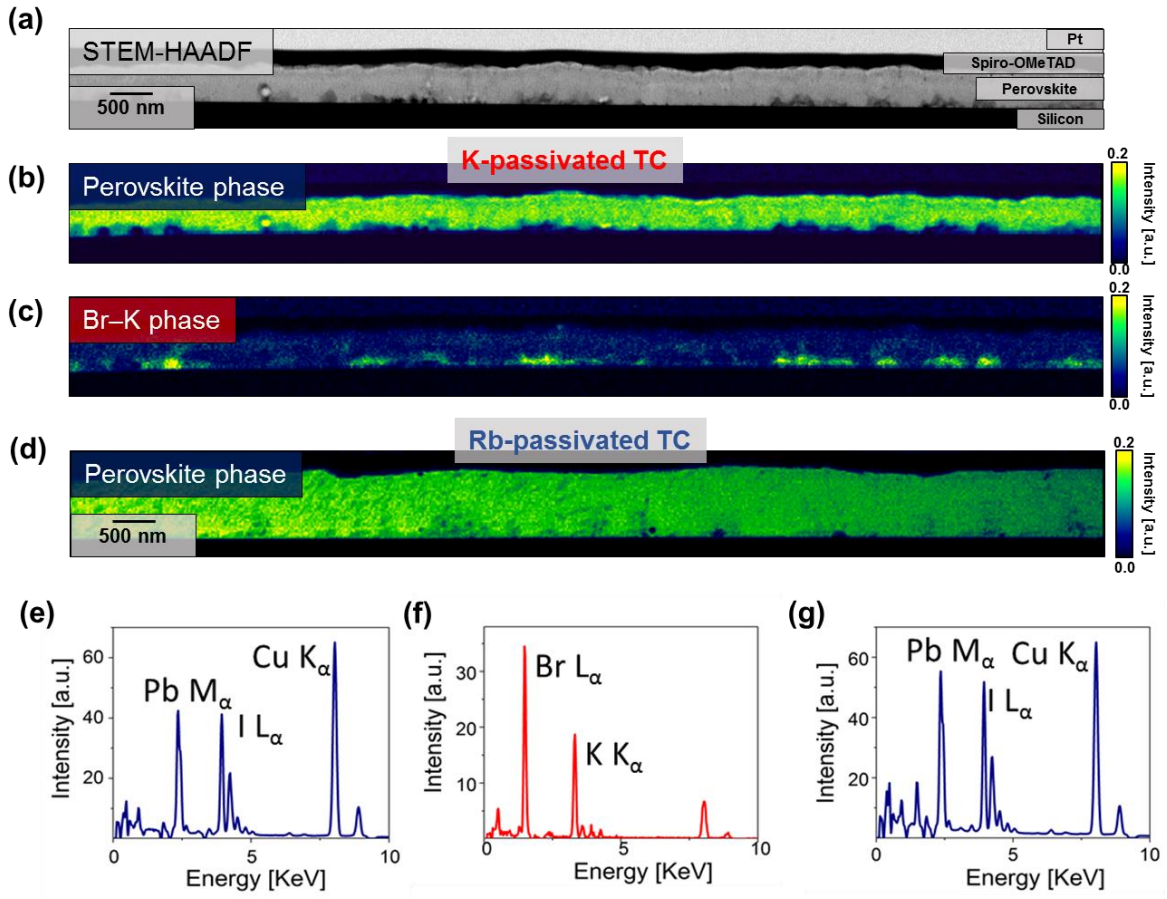

Figure S5. (a) HAADF STEM cross sectional image of a TC perovskite thin film passivated with x = 0.10 of potassium (K). NMF decomposition of K-passivated TC results showing the (b) perovskite phase (corresponding EDX spectra in e) and (c) K-Br phase (corresponding EDX spectra in f). (d) NMF decomposition of Rb-passivated TC showing the perovskite phase (corresponding EDX spectra in g).

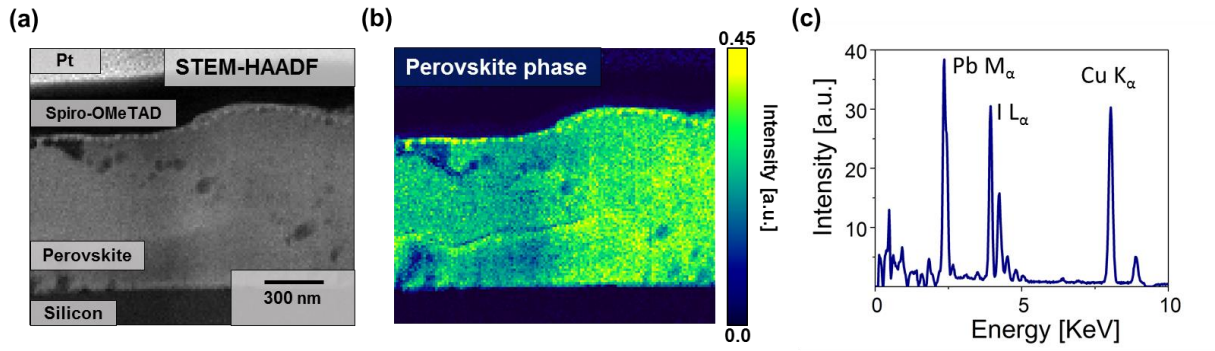

Figure S6. (a) HAADF STEM cross sectional image, (b) intensity plot and (c) elemental profile for Rb-passivated TC perovskite phase from NMF decomposition analyses.

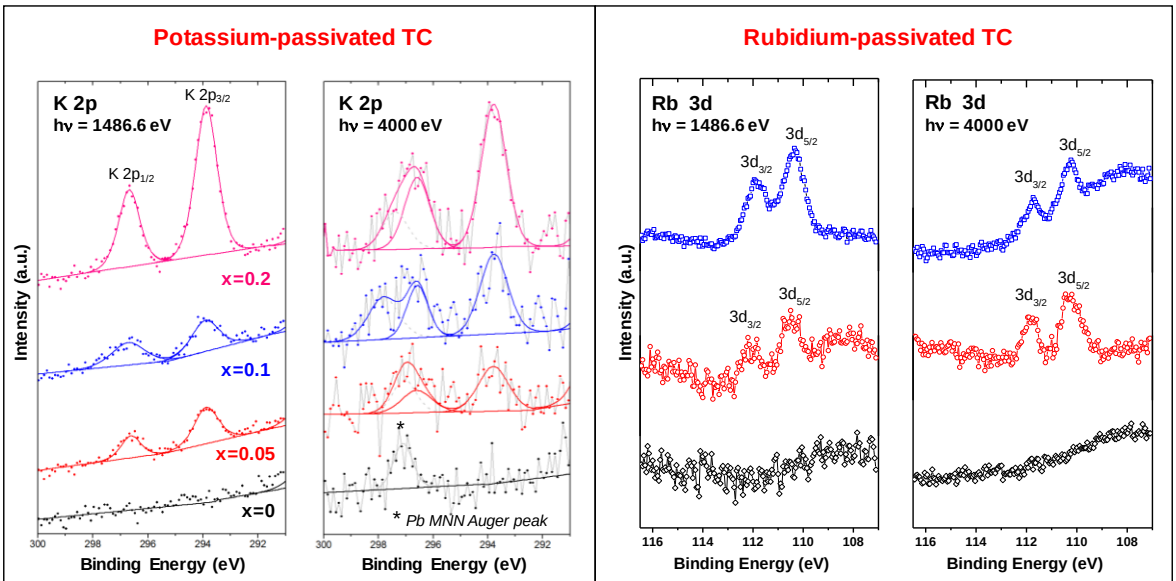

K/Pb intensity ratio	x = 0.05	x = 0.10	x = 0.20
1486.6 eV	0.035	0.061	0.12
4000 eV	0.011	0.025	0.046

Rb/Pb intensity ratio	x = 0.05	x = 0.10
1486.6 eV	0.033	0.052
4000 eV	0.031	0.057

Figure S7. XPS (1486.6 eV) and HAXPES (4000 eV) spectra of the K 2p and Rb 3d core levels. Atomic ratios are quantified via the spectra for potassium- (left panel) and rubidium-passivated (right panel) triple cation perovskite.

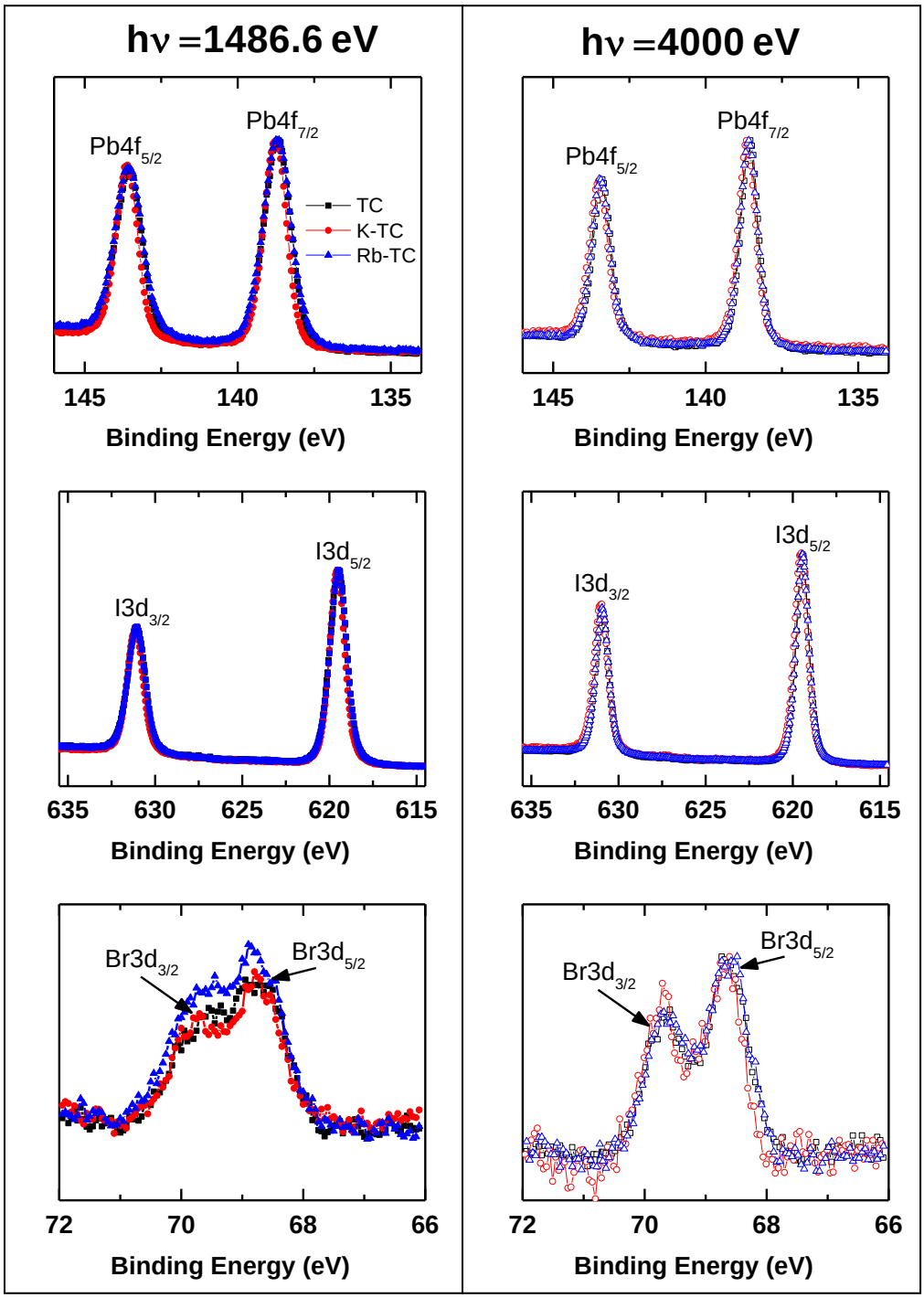

Figure S8. Pb 4f, I 3d and Br 3d XPS (1486.6 eV) and HAXPES (4000 eV) core level spectra of the pristine (TC), potassium- (K-TC) and rubidium-passivated (Rb-TC) alloyed perovskites.

Table S2. Summary of quantitative analysis on the NMF components that are rich in additives (i.e. K and Rb) extracted from the STEM-EDX results. Note that due to the convolution of the signal from this phase from the surrounding signal (due to several phenomena, including absorption and fluorescence) the measurement provides an estimate with a confidence of a few atomic percent points.

Atoms	Rb-passivated TC (atomic%)	K-passivated TC (atomic%)
Rb_Ka	18	-
K_Ka	-	28
Pb_La	1.4	0.5
I_La	38	3
Br_Ka	5	28
C_Ka	10	11

In Figure S9, we show the PL spectra of the triple cation perovskite films with different loadings of rubidium and potassium. In both cases, the PL peak is red-shifted with increasing fraction of additives relating to the changes in the halide ratio in the perovskite lattice (I/Br; i.e. this ratio increases). The more pronounced red-shift of PL for potassium passivation is consistent with the increased interaction between potassium and bromide and formation of bromide-rich species, in turn leading to lower content of Br in the perovskite lattice.

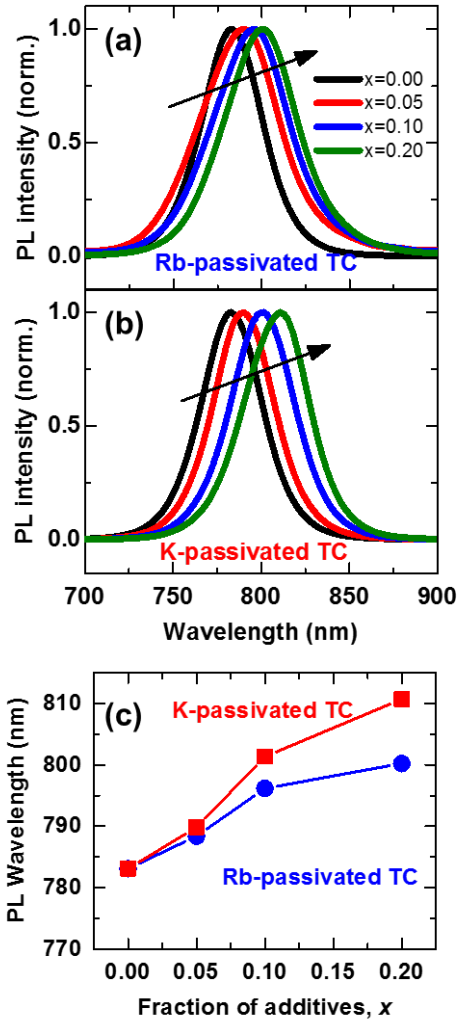

Figure S9. Photoluminescence spectra of (a) rubidium-passivated and (b) potassium-passivated TC with different fraction of Rb and K measured using 532-nm continuous-wave excitation. (c) The PL peak wavelength of passivated perovskite thin films extracted from a and b.

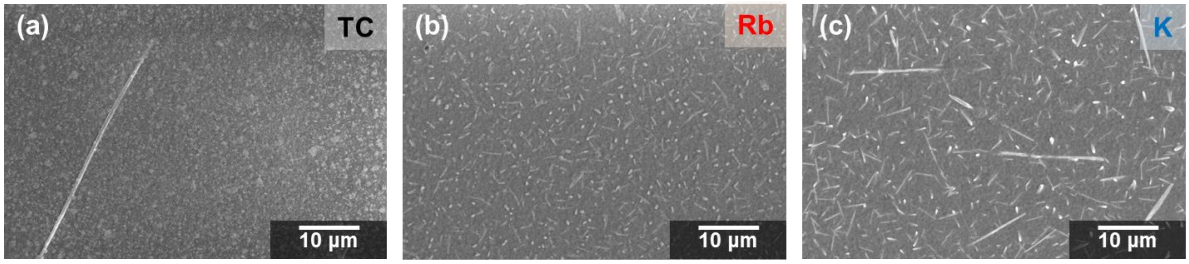

Figure S10. Top view zoomed-out SEM images of (a) TC, (b) Rb-doped TC and (c) K-doped TC perovskite thin films exposed to 50% RH for 24 hours.

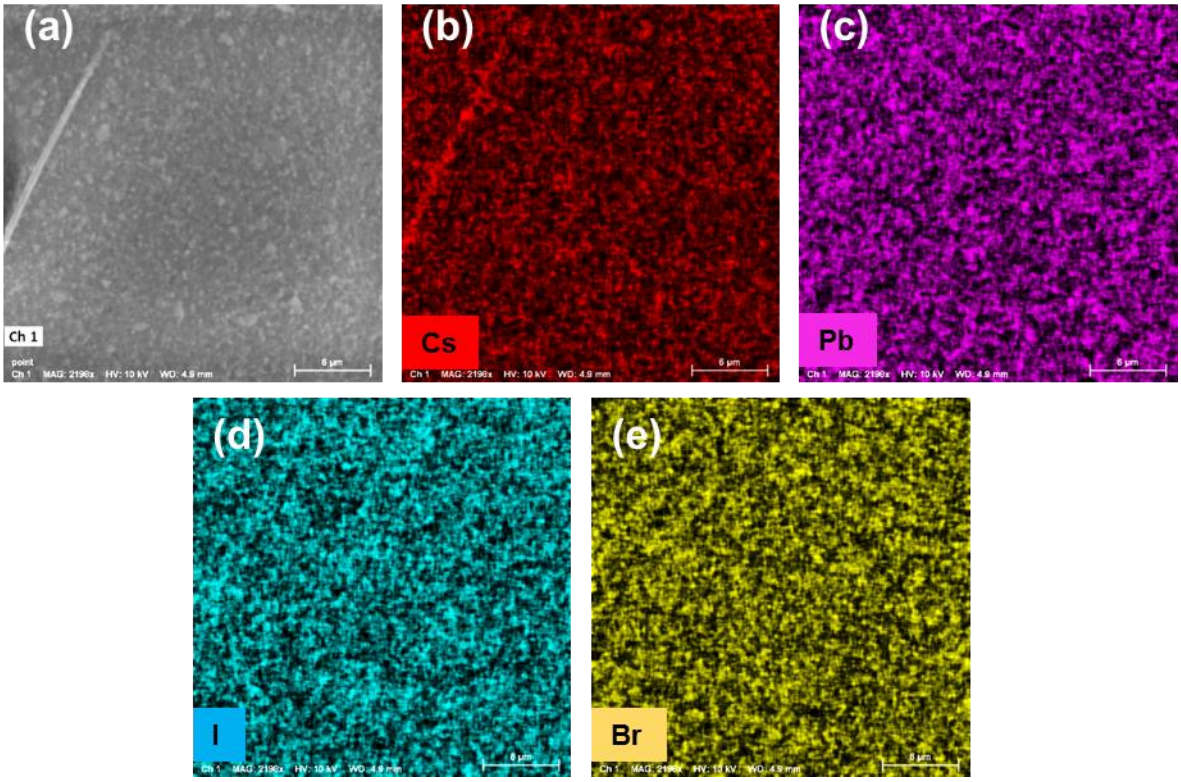

Figure S11. (a) Top view SEM image of TC perovskite and the corresponding SEM-EDX elemental maps of (b) Cs, (c) Pb, (d) I and (e) Br, measured after humidity exposure to 50% RH (N_2) for 24 hours.

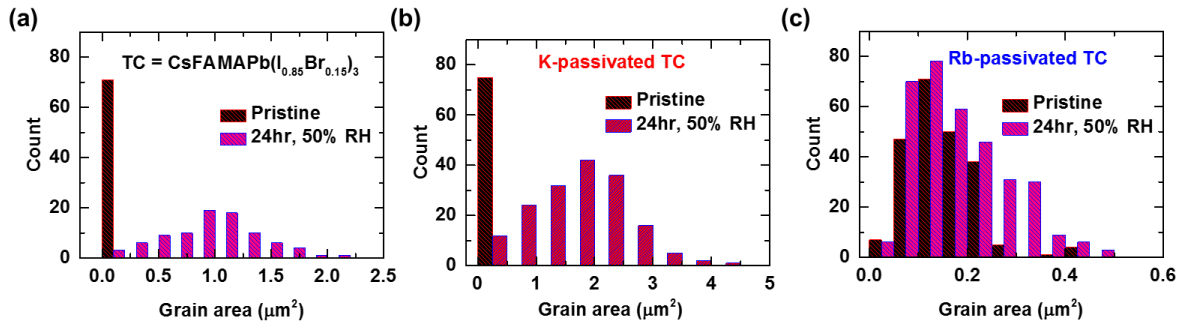

Figure S12. **Grain area distributions**. Histogram of the grain areas for (a) TC, (b) K-passivated TC and (c) Rb-passivated TC films before (pristine) and after 24hr humidity exposure (50%, N_2) extracted from analyses of the SEM images (Figure 4) using ImageJ software.

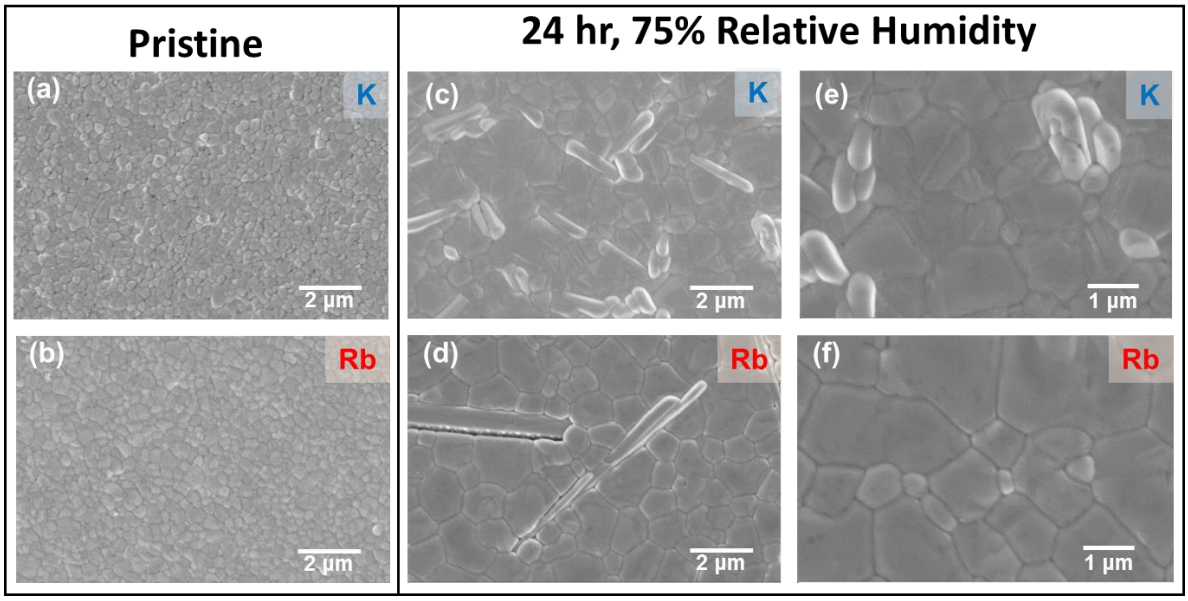

Figure S13. Top view SEM images of the K- and Rb-doped perovskite thin films (a, b) before exposure (pristine) and (c-f) after exposure to 75% RH at different magnifications.

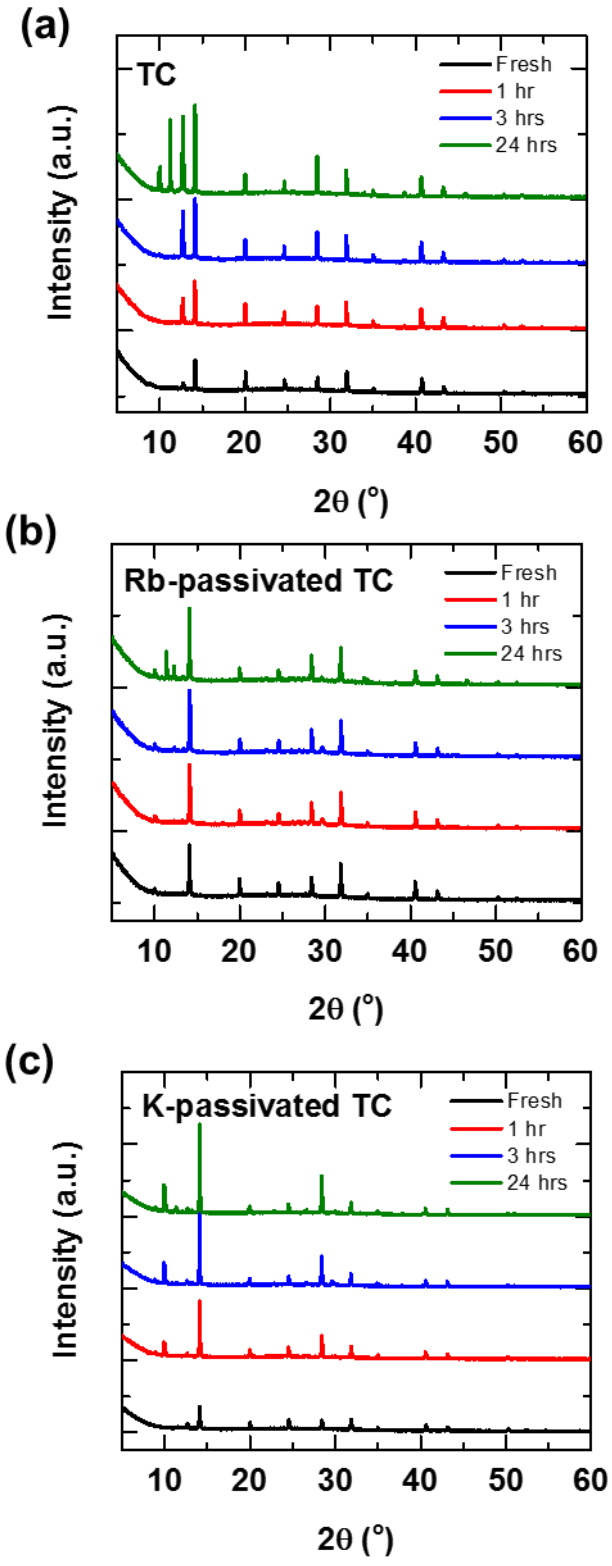

Figure S14. Full XRD patterns of (a) TC, (b) Rb-doped TC and (c) K-doped TC films measured fresh (pristine) and after different exposure time to nitrogen with 50% RH.

Supporting References

1. Abdi-Jalebi, M.; Andaji-Garmaroudi, Z.; Cacovich, S.; Stavrakas, C.; Philippe, B.; Richter, J. M.; Alsari, M.; Booker, E. P.; Hutter, E. M.; Pearson, A. J.; Lilliu, S.; Savenije, T. J.; Rensmo, H.; Divitini, G.; Ducati, C.; Friend, R. H.; Stranks, S. D., Maximizing and stabilizing luminescence from halide perovskites with potassium passivation. *Nature* **2018,** *555* (7697), 497-501.

2. Abdi-Jalebi, M.; Dar, M. I.; Sadhanala, A.; Senanayak, S. P.; Giordano, F.; Zakeeruddin, S. M.; Grätzel, M.; Friend, R. H., Impact of a Mesoporous Titania–Perovskite Interface on the Performance of Hybrid Organic–Inorganic Perovskite Solar Cells. *The Journal of Physical Chemistry Letters* **2016,** *7* (16), 3264-3269.

3. de Mello, J. C.; Wittmann, H. F.; Friend, R. H., An improved experimental determination of external photoluminescence quantum efficiency. *Adv. Mater.* **1997,** *9* (3), 230-232.

4. Abdi-Jalebi, M.; Pazoki, M.; Philippe, B.; Dar, M. I.; Alsari, M.; Sadhanala, A.; Divitini, G.; Imani, R.; Lilliu, S.; Kullgren, J.; Rensmo, H.; Grätzel, M.; Friend, R. H., Dedoping of Lead Halide Perovskites Incorporating Monovalent Cations. *ACS Nano* **2018,** *12* (7), 7301-7311.